ADVANCED ELECTRONIC MATERIALS
www.advelectronicmat.de

Charge Transfer Doping of 2D $PdSe_2$ Thin Film and Its Application in Fabrication of Heterostructures

*Sajeevi S. Withanage, Bhim Chamlagain, Ammon C. Johnston, and Saiful I. Khondaker**

Palladium diselenide ($PdSe_2$) is an emerging 2D material with exotic optical and electrical properties and widely tunable layer dependent band gap in the infrared regime. The ability to further tune the electronic properties of $PdSe_2$ via doping is of fundamental importance for a wide range of electronic and optoelectronic device applications. Here, surface charge transfer doping of chemical vapor deposition grown p-type $PdSe_2$ thin film using benzyl viologen (BV) molecules is reported. The electrical transport measurements of the $PdSe_2$ device show an increase in resistance by ≈1700 percent from 2.1 MΩ for the pristine sample to 36.2 MΩ upon BV doping, revealing electrons are transferred from BV molecules to $PdSe_2$ resulting in an n-doping. Raman characterization shows a red-shift and broadening of A^3_g characteristic peak for the doped sample, while X-ray photoelectron spectroscopy shows a negative shift in Pd 3d and Se 3d binding energies confirming n-doping by BV. Kelvin force probe microscopy measurements show a ≈0.3 eV decrease in work function for doped $PdSe_2$, consistent with the n-doping by BV molecules. A selective doping of $PdSe_2$ channel is implemented for the fabrication of lateral heterojunction device which shows good current rectifying behavior with a rectification ratio of up to ≈55.

1. Introduction

Atomically thin transition metal dichalcogenides (TMDs) are receiving significant attention due to their extraordinary structural, optical, electrical, and mechanical properties which are significantly different from their bulk counterparts. Group-VI TMDs such as molybdenum disulfide (MoS_2), tungsten disulfide (WS_2), etc. are extensively studied for device applications owing to their high photoresponse,[1] high on/off ratios,[2] appreciable carrier mobilities,[2] and high flexibility.[3] However, the intrinsic band-gaps of these materials show a limited variation[2,4] that falls mostly in the visible wavelength regime and band-gap tunability can only be achieved for up to a few layers. While black phosphorus (BP), a narrow band-gap semiconductor with a widely tunable band-gap from 0.3 to 2 eV,[5,6] can bridge the energy gap between the TMDs and zero-bandgap graphene for near infrared, mid infrared (IR) applications,[5,7] it is highly unstable in air which significantly limits its application in practical electronic and optoelectronic devices.

In recent years, there is a growing interest in group-X noble TMDs such as platinum diselenide, platinum disulfide and palladium diselenide ($PdSe_2$) due to their excellent air stability and widely adjustable band gaps similar to BP. In particular, $PdSe_2$ is a recently discovered material in which Pd atom bonds with four Se atoms to form the basic tetragonal unit of the lattice and these units are connected to form waved layers via Se—Se bonds giving its unique puckered pentagonal structure to $PdSe_2$.[8] $PdSe_2$ is the first air-stable 2D material isolated that compose of such pentagonal structure with vertical puckering distance of 1.6 A.[6] The added degree of freedom in the puckered structure and low symmetry of the pentagonal lattice have shown exciting anisotropic electrical and optical phenomena in 2D $PdSe_2$.[6,9] The bandgap of $PdSe_2$ can be varied from near 0 eV (quasi-metallic) in bulk to 1.3 eV in monolayer. Unlike in MoS_2, where the band gap reaches its bulk value within 5–6 layers,[10] the band gap of $PdSe_2$ can be controlled more continuously with the layer number up to 40+ layers[11] which makes them very promising for high performance electronic and optoelectronic devices such as photodetectors operating in wide range of IR wavelengths.[12,13]

In addition to the inherent layer dependent electrical properties, the ability to further tune the electrical properties of $PdSe_2$ via controlled doping is of fundamental importance for their wide range of electronic and optoelectronic device applications. Although a large number of first principle theoretical studies are initiated in recent years[14] due to the evolving interest in the versality of electrical, magnetic, and optical properties that could be induced by doping of these materials, practical demonstration of doping engineering of $PdSe_2$ and other group-X TMDS is still at its infancy.[25] Surface charge transfer doping (SCTD) is a simple, reliable, and non- destructive method to achieve efficient doping in semiconductor materials.[15,16] In

S. S. Withanage, Dr. B. Chamlagain, A. C. Johnston, Prof. S. I. Khondaker
NanoScience Technology Center
University of Central Florida
Orlando, FL 32826, USA
E-mail: saiful@ucf.edu

S. S. Withanage, A. C. Johnston, Prof. S. I. Khondaker
Department of Physics
University of Central Florida
Orlando, FL 32816, USA

Prof. S. I. Khondaker
Department of Electrical and Computer Engineering
University of Central Florida
Orlando, FL 32816, USA

The ORCID identification number(s) for the author(s) of this article can be found under https://doi.org/10.1002/aelm.202001057.

DOI: 10.1002/aelm.202001057

charge transfer doping, dopant molecules adsorbs on the surface of semiconductor material and exchange charges to dope the material. SCTD could be particularly effective in 2D materials owing to their high surface to volume ratio and exposed basal planes which enhance the surface adsorption of dopant molecules.[17] Successful utilization of SCTD to modulate electrical properties in chemical vapor deposition (CVD) grown $PdSe_2$ could be a significant step toward its integration in practical applications.

Here, we report an effective SCTD of CVD grown $PdSe_2$ thin film samples using BV molecules. $PdSe_2$ channels were grown via low pressure selenization of patterned Pd film at 325 °C. The FET fabricated on pristine $PdSe_2$ showed p-type conduction with a mobility of 0.58 $cm^2\ V^{-1}\ s^{-1}$ and resistance of 2.1 MΩ. Adsorption of BV molecules effectively lowered hole concentration in the $PdSe_2$ channel due to the transfer of electrons from BV via SCTD resulting in a large increase in resistance to 36.2 MΩ and a decrease in mobility to 0.44 $cm^2\ V^{-1}\ s^{-1}$. Raman analysis showed that A^3_g peak red-shifted by 1.2 cm^{-1} and broadened by 2.1 cm^{-1} confirming the n-doping of the $PdSe_2$ film by BV. Electron transfer from BV to $PdSe_2$ was further confirmed by X-ray photoelectron spectroscopy (XPS) where binding energies (BEs) of Pd 3d and Se 3d core levels showed a negative shift with respect to the pristine material. Effective work function (WF) modulation of $PdSe_2$ with BV doping was observed via Kelvin probe force microscopy (KPFM) measurements where the n-doping caused a 0.3 eV decrease in WF of BV doped $PdSe_2$. We successfully applied the carrier density and WF modulation of $PdSe_2$ by SCTD to fabricate lateral heterojunction devices. Excellent current rectifying behavior was observed in the heterojunction devices with a maximum rectification ratio of ≈55.

2. Results and Discussions

The $PdSe_2$ thin films were grown via selenization of predeposited Pd thin films on Si/SiO_2 substrates using low pressure chemical vapor deposition (LPCVD) technique as described in Section 4. The LPCVD setup and optical images of a Pd film before and after selenization process can be found in the supporting information (Figure S1, Supporting Information). After selenization, a noticeable color change of the film from pink to metallic gray was observed (Figure S1b, Supporting Information) suggesting the transformation of Pd to $PdSe_2$. The AFM image show initial thickness of Pd to be 2 nm (Figure S2a, Supporting Information), which transforms to a uniform $PdSe_2$ film with a thickness of 8 nm (**Figure 1**a) after selenization corresponding to a 20 layer (L) of $PdSe_2$.[11] This thickness expansion is in good agreement with previously reported data for $PdSe_2$ grown via similar selenization method.[11] The polycrystalline nature of the film was observed in the small area AFM scan shown in Figure S2b, Supporting Information, with average grain size of ≈15 nm and rms roughness of ≈0.4 nm. Raman measurement was used to further confirm the formation of $PdSe_2$. The Raman single spectra shown in Figure 1b show four prominent peaks at 146, 208.4, 224.1, and 258.8 cm^{-1} for our sample which corresponds to A^1_g, A^2_g, B^2_{1g}, and A^3_g vibrational peaks of $PdSe_2$, respectively. Theoretically, $PdSe_2$ Raman spectra is expected to show six prominent peaks due to 3 A_g (A^1_g, A^2_g, A^3_g) and 3 B_{1g} (B^1_{1g}, B^2_{1g}, B^3_{1g}) vibrational modes in the $PdSe_2$ lattice.[6] However, A^1_g/B^1_{1g} and A^3_g/B^3_{1g} peaks are located very close together, therefore often observed as single peaks. The observed values of Raman peaks are consistent with previous reports of 2D $PdSe_2$.[11,12] For electrical characterizations, patterned $PdSe_2$ thin films of 200 µm × 30 µm were grown using a shadow mask. Drain and source electrodes were defined by depositing Au contacts through a shadow mask for the pre-defined $PdSe_2$ channel with dimensions of L = 100 µm and W = 30 µm. FET device properties were measured in ambient conditions by using highly doped silicon as the gate electrode and 250 nm thick SiO_2 as the gate dielectric. The linear current–voltage (I–V) characteristics curve shown in Figure 1c suggests that the Au electrodes are making Ohmic contacts with the $PdSe_2$ channel. The gate voltage (V_g) was fixed at 0 V. The drain current at 1 V was measured to be 0.48 µA and the device resistance was calculated to be 2.1 MΩ. The I–V_g curve of the same device is shown in the bottom-right inset. The increase of the current with decrease of the gate voltage indicates p-type transport behavior of the $PdSe_2$ FET device. The field effect mobility of the device was calculated to be 0.58 ± 0.02 $cm^2\ V^{-1}\ s^{-1}$ using the equation

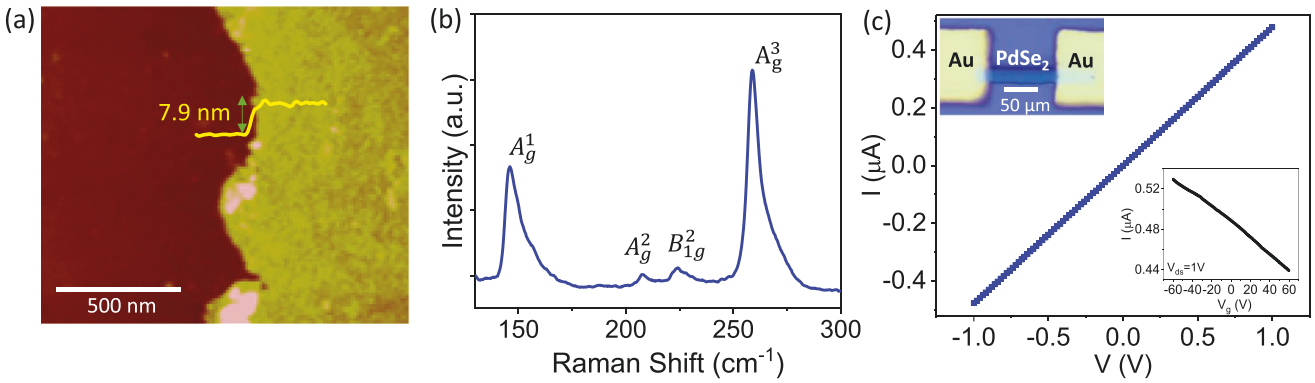

Figure 1. Characterizations of a pristine $PdSe_2$ device. a) AFM topography and height profile of a Pd film after selenization. b) Raman spectra of a $PdSe_2$ sample showing characteristics peaks, c) I–V characteristics of a $PdSe_2$ device (V_g = 0 V). The inset in top-left is an optical image and the bottom-right inset shows the transfer characteristics of the device.

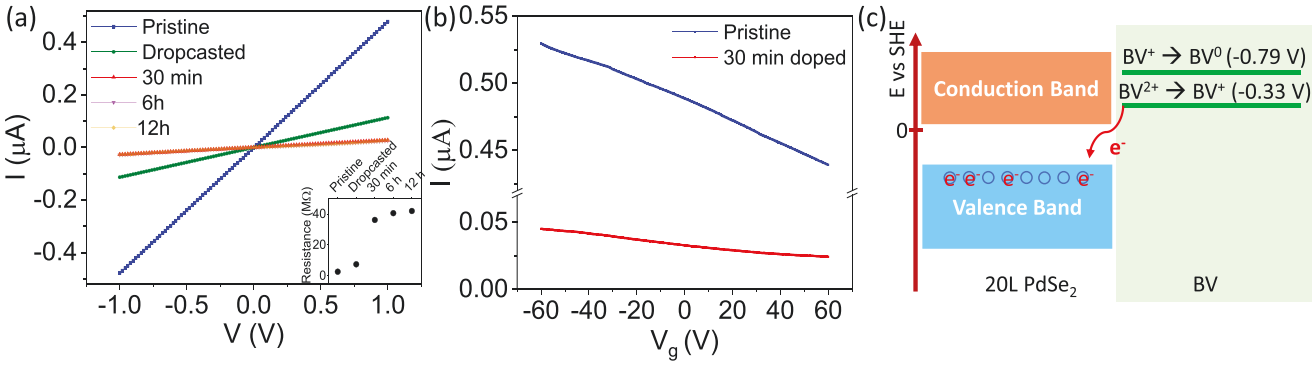

Figure 2. BV doping of a $PdSe_2$ device. a) *I–V* characteristics of a pristine and BV doped $PdSe_2$ device with different BV exposure time. The inset shows the resistance variation of the device. b) Transfer characteristics of the pristine and 30 min BV doped device. c) Schematic illustration to show the charge transfer process between $PdSe_2$ and BV.

$\mu = (L/WC_gV_{ds}) \times (dI/dV_g)$, where L, W, and C_g are the channel length, width, and the capacitance per unit area of gate dielectric, respectively. The relatively lower mobility of the device compared to the exfoliated sample with similar thickness[6] is possibly caused by the polycrystalline nature of the film and is consistent with the mobilities reported for similar polycrystalline $PdSe_2$ and other 2D TMD films.[18]

We tested the SCTD effect on the conductivity of the $PdSe_2$ FET device with BV immersion time and the results are shown in **Figure 2**. First, we drop casted a small amount of BV solution on $PdSe_2$ device and measured the *I–V* characteristics after drying the solution. The device was then immersed in BV solution for 30 min and measured again. The process was repeated by immersing the sample in BV solution for additional 5.5 h (total of 6 h) followed by another 6 h (total of 12 h). As illustrated from the *I–V* curves (Figure 2a and Figure S3, Supporting Information) the device conductivity is strongly affected by BV doping. The drain current of the device measured at 1 V was decreased to 0.11 μA after drop-casting BV and 0.03 μA after 30 min doping. With longer BV immersion time, the change in the drain current is hardly noticeable in the *I–V* curve (Figure S3, Supporting Information). The inset of Figure 2a shows the resistance variation of the device as a function of BV immersion time. The $PdSe_2$ devices showed increase of resistance to 7.5 MΩ when BV solution is drop-casted on the sample. After 30 min immersion of the devices in BV solution, the average resistance increased to 36.2 MΩ which is ≈1700 percent higher compared to the resistance of pristine device. The resistance of the device was measured to be 40.6 and 42 MΩ after 6 and 12 h immersion time. Therefore, the sample was close to saturation of doping in 30 min. Similar trend was observed in multiple other devices measured and the resistance variation of two other devices are shown in Figure S4, Supporting Information. We also observed relatively smaller drain current variation with gate voltage in the transfer curve shown in Figure 2b after doping as compared to pristine $PdSe_2$ device. In the pristine device, the average slope of $I–V_g$ curve was calculated as -7.5×10^{-4} μA and in the BV doped device it is decreased to -1.8×10^{-4} μA. The field effect mobility after 30 min doping was calculated to be 0.44 ± 0.02 cm^2 V^{-1} s^{-1}. Comparing the 20 L thickness of the pristine $PdSe_2$ film to the layer dependent band-gap reported in the literature, we anticipate that the valence and conduction bands are located around the energy values of –4.4 and –5.1 eV.[11] Accordingly, the conduction band edge of $PdSe_2$ stays very close to the 0 V versus SHE.[19] Hence, based on the previously reported redox potentials for BV[16,20] (–0.79 V vs standard hydrogen electrode (SHE) for BV^0/BV^+ and –0.33 V vs SHE for BV^+/BV^{2+}, respectively) and the conduction band minimum (CBM) and valence band maximum (VBM) for 20 L $PdSe_2$,[11] we can depict energy diagram of the few layer $PdSe_2$ and BV as shown in Figure 2c. According to this diagram, the BV reduction potential is at a higher energy than the VBM and CBM of $PdSe_2$. Therefore, electron transfer from BV to $PdSe_2$ is expected. Upon electron transfer, the hole concentration in the valence band decreases resulting in an increase of resistance and decrease in carrier mobility.

Based on the charge transfer model depicted in Figure 2c, each BV molecule adsorbed on the surface can donate 2 electrons to $PdSe_2$ and these electrons can then diffuse to the inner layers of the sample. For $PdSe_2$ film, which is polycrystalline in nature, the molecules can diffuse through the grain boundaries to the bottom layers effectively.[21] The number of electrons transferred to $PdSe_2$ is limited by effective area of exposure to BV molecules. When more BV^{2+} are adsorbed on the $PdSe_2$ surface, further BV molecules cannot be adsorbed on the $PdSe_2$ surface for additional charge transfer. As a result, even after 12 h immersion of $PdSe_2$ devices into the BV solution, $PdSe_2$ did not show electron dominant transport. Similar behavior was observed previously in n-type monolayer WS_2 doped with strong electron accepting molecule F4-TCNQ in which electron concentration gradually decreased and subsequently saturated with doping time while preserving the n-type conduction of the channel.[22]

It is known that the Raman peak position and FWHM of the out-of-plane vibrational modes are sensitive to doping. Raman spectra of the pristine and BV doped $PdSe_2$ sample is shown in **Figure 3**a. We observed that all the peaks are red-shifted and broadened upon doping, these changes are more significant in the highest intensity A^3_g peak. The A^3_g peak of the BV doped sample is located at 257.6 cm^{-1} which is a 1.2 cm^{-1} shift toward lower wavenumbers compared to the pristine sample. The FWHM of the A^3_g peak is also increased from 7.1 cm^{-1} (pristine)

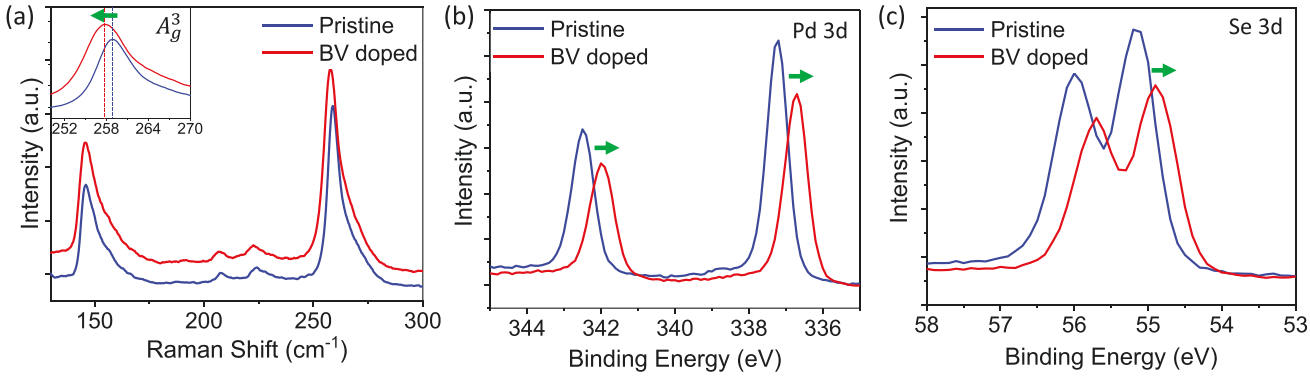

Figure 3. Raman and XPS characterization of a BV doped $PdSe_2$ sample. a) Raman spectrum for pristine and BV doped $PdSe_2$. The inset shows a close-up view of the spectra at A^3_g peak location. b) Pd 3d and c) Se 3d XPS core level spectra of a pristine (blue) and BV doped (red) $PdSe_2$ film, respectively.

to 9.2 cm^{-1} after doping. The electrons transferred to $PdSe_2$ from BV increases the electron–phonon coupling in the lattice causing phonon softening which resulted in red-shift and broadening of the peaks. No additional peaks appeared in the spectra after doping indicates that the chemical composition of the film is not altered by the doping, this non-destructive nature is a main advantage of SCTD of 2D materials.[15] We further characterized the samples via XPS to verify the surface chemical composition and changes to the electronic structure after BV doping. The Pd 3d and Se 3d core level spectra for the pristine and BV doped $PdSe_2$ samples are shown in Figure 3(b,c), respectively. The pristine sample (blue) show Pd $3d_{5/2}$, Pd $3d_{3/2}$ peaks at 337.2 and 342.5 eV, and Se $3d_{5/2}$, Se $3d_{3/2}$ peaks at 55.2 and 56 eV, respectively which are consistent with the characteristic peak positions for $PdSe_2$.[23] After BV doping (red), we observed the Pd 3d peaks shifted by 0.5 eV, while Se 3d peaks shifted by 0.3 eV toward lower BE. This BE shift provides a fundamental understanding to the charge transfer process between BV molecules and $PdSe_2$ which resulted in a decrease in hole charge carriers in the valence band of $PdSe_2$ observed in electrical characterizations. XPS studies can identify the BE of elements shift upon electron occupation (donation) due to the increased (decreased) intra-atomic electron–electron repulsion, a negative BE shift is observed with occupation of electrons and positive BE shift is correlated with electron donation.[24] Therefore, the negative shift in the core level spectra observed in our study is an indication that electrons are transferred from BV to $PdSe_2$[25] and is consistent with our electrical transport and Raman study. The electron transfer from BV places more electron density into the valence band and they localize at Pd/Se sites decreasing their core-level BEs.

To investigate the WF change in $PdSe_2$ due to BV doping, we conducted KPFM measurements on both pristine and BV doped samples. The mapping shown in **Figure 4** corresponds to the contact potential difference (CPD) between the gold coated KPFM probe and the sample. Highly oriented pyrolytic graphite (HOPG) with WF of 4.6 eV[26] was used as the reference material to calibrate the probe in order to measure the WFs of the samples. The KPFM mapping of the pristine $PdSe_2$ sample is shown in Figure 4a while the mapping for BV doped samples is shown in Figure 4b. We measured an average CPD to be –71 ± 10 mV for the pristine sample and 240 ± 20 mV for the BV doped sample. The WFs are calculated using the equation $V_{CPD} = \frac{\phi_{tip} - \phi_{sample}}{e}$ where V_{CPD} is the CPD in volts, ϕ_{tip} is the WF of the tip, ϕ_{sample} is the WF of the sample and e is the electron charge. With the HOPG calibration, ϕ_{tip} was found to be 4.81 ± 0.01 eV. The WFs of the pristine sample was calculated to be 4.88 ± 0.02 eV. This WF is consistent with the anticipated VBM (–5.1 eV) and CBM (–4.4 eV) discussed earlier for 20 L $PdSe_2$ since it shows that the Fermi level stays closer to the valence band of the intrinsic p-type $PdSe_2$. The WF of BV doped film was calculated as 4.57 ± 0.03 eV, the WF lowering by ≈0.3 eV after BV doping further confirms that BV molecules donated electrons (n-doping) to the $PdSe_2$ film.[26,27]

To show an application of the $PdSe_2$ WF modulation via BV doping, we fabricated lateral heterojunction devices by implementing selective area doping of a $PdSe_2$ channel. For selective area BV doping and heterojunction fabrication, we used the poly-methyl methacrylate (PMMA)/metal mask patterning technique[28] shown schematically in **Figure 5**a. First, the $PdSe_2$ devices were fabricated as described in Section 4. Then the substrate was spin coated with PMMA followed by Au deposition through a shadow mask which was aligned to cover half of the $PdSe_2$ channel. After the Au deposition, the sample was exposed to oxygen plasma to etch the PMMA that was not covered by gold to partially expose the $PdSe_2$ thin film for BV doping. The substrate was then immersed in the BV solution for 30 min. This allowed the uncovered area of the $PdSe_2$ channel to dope while covered area remained undoped. As a result, a heterojunction is created between doped and undoped section of the $PdSe_2$ channel. *I–V* characteristics of a representative

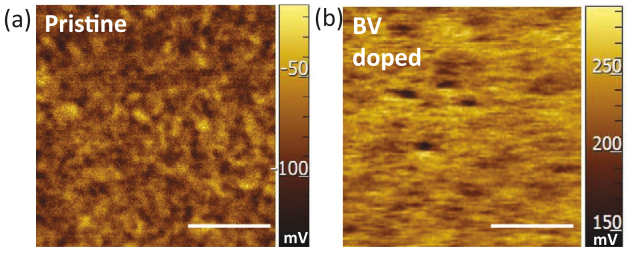

Figure 4. KPFM contact potential mapping of a) pristine and b) BV doped $PdSe_2$. Scale bar is 1 µm in each image.

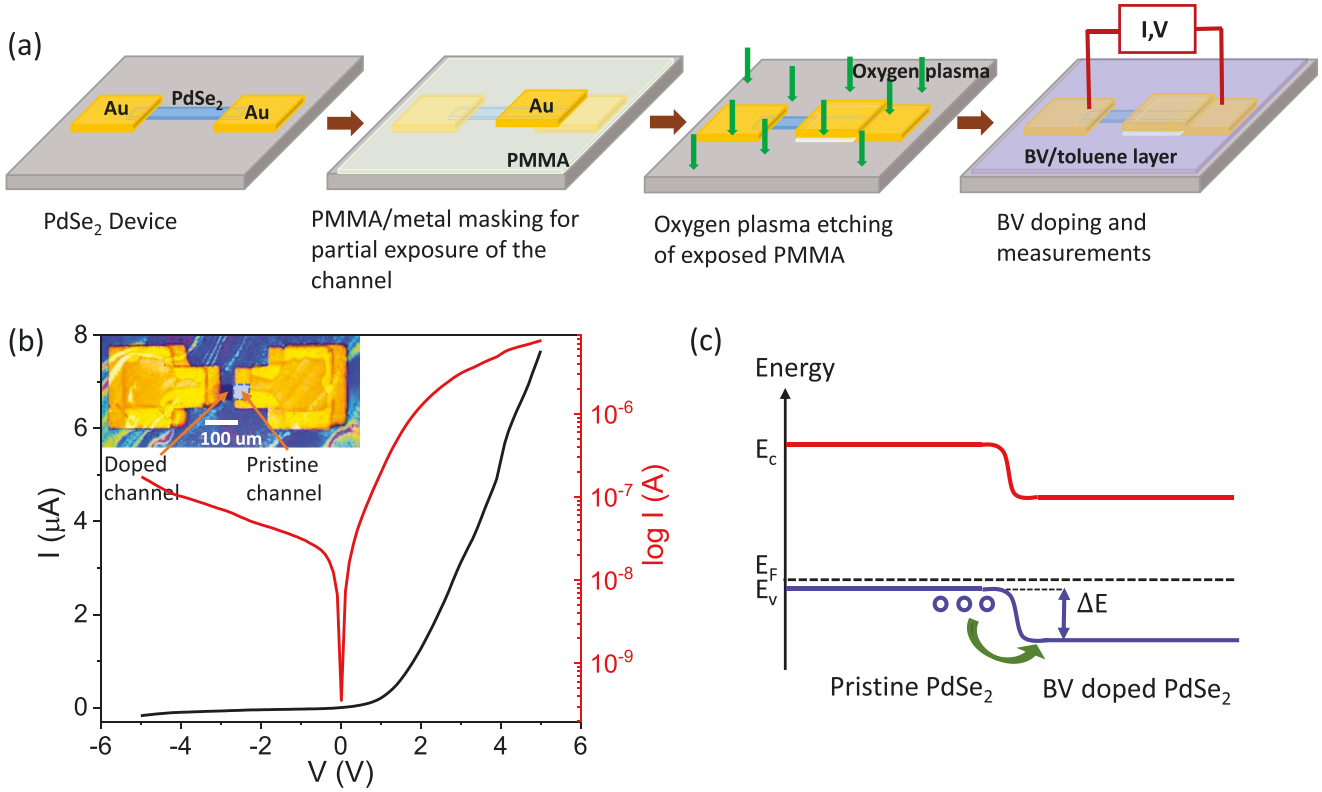

Figure 5. a) Schematic diagrams showing the fabrication steps of $PdSe_2$ lateral heterojunctions by selective BV doping. b) *I–V* characteristics of a heterojunction device in linear scale (black) and log scale (red). The inset shows an optical image of the device. c) An illustration of the band offset with energy barrier (ΔE) created at the junction between pristine and BV doped $PdSe_2$.

heterojunction device are shown in Figure 5b. The *I–V* characteristics of the device show a diode-like behavior (black curve) confirming that a heterojunction has been formed. Breakdown of the $PdSe_2$ heterojunction device was not observed until −5 V. The rectification ratio for the device was calculated by the ratio of $I_{forward}/I_{reverse}$ for the range of voltage in the *I–V* curve and the maximum rectification ratio was found to be ≈55. To verify that this rectification behavior is solely an effect of BV doping, we conducted *I–V* measurements in each fabrication steps (Figure S5b, Supporting Information). We observed linear *I–V* curves with similar current values indicating that the rectification behavior is not due to fabrication steps before doping. Therefore, the rectifying behavior is exclusively a consequence of the band offset occurred at the junction of pristine and BV doped $PdSe_2$. The KPFM study shows the work function of pristine and BV doped $PdSe_2$ to be 4.88 and 4.57 eV, respectively. This leads to a band offset at the junction of pristine and BV doped $PdSe_2$ as shown in Figure 5c. This band offset allows the flow of charge carriers in forward bias while preventing the flow in reverse bias leading to a diode like behavior.

3. Conclusion

In conclusion, we demonstrated an effective SCTD of 2D $PdSe_2$ thin films by using BV molecules. Patterned $PdSe_2$ samples were obtained by low pressure selenization of a pre-deposited Pd film. Pristine $PdSe_2$ device showed p-type conduction with a mobility of 0.58 $cm^2\ V^{-1}\ s^{-1}$ and average resistance of 2.1 MΩ. $A \approx 1700$ percent increase in resistance and a decrease in mobility to 0.44 $cm^2\ V^{-1}\ s^{-1}$ was observed due to n-doping of $PdSe_2$ by BV molecules. Raman and XPS characterizations further confirmed the decrease in carrier concentration in doped sample is due to the electron transfer from BV to $PdSe_2$ (n-doping). KPFM measurements showed that the WF of $PdSe_2$ was effectively modulated by BV doping, a decrease of ≈0.3 eV in the WF of $PdSe_2$ was measured after doping. A selective doping was implemented for the fabrication of heterojunction between pristine and BV doped $PdSe_2$, which showed good current rectification behavior with a rectification ratio of up to ≈55 demonstrating the importance of SCTD to modify electrical properties of the $PdSe_2$. The facile, non-destructive doping method we discussed here can be used toward fabrication of high performance $PdSe_2$ electronic devices.

4. Experimental Section

$PdSe_2$ Film Growth: Patterned $PdSe_2$ channels were grown via low pressure selenization of pre-deposited Pd channels on Si/SiO_2 substrate (250 nm of SiO_2 thickness) in a CVD tube furnace. Prior to Pd deposition, substrates were cleaned by sonicating in acetone and isopropanol for 5 min followed by deionized water rinse and nitrogen blow drying. Cleaned substrates were treated in mild oxygen plasma for 10 min to further remove the organic residue. The substrate was then covered with a shadow mask with defined channels of 30 μm × 200 μm and 2 nm thick Pd film was deposited via e-beam deposition

in a vacuum chamber at an evaporation rate of ≈ 0.5 A s^{-1}. Thickness of the film was confirmed by AFM height measurements. Thin film deposited substrate was then placed at the center of a 1-inch quartz tube in a single zone tube furnace (Barnstead International F79300 Tube Furnace). Ceramic crucible containing 2 g of Se powder (99.5%, Sigma Aldrich) was placed upstream at the edge of the heating zone in such a way that Se started melting when the temperature at the center of the furnace reached 250 °C. The quartz tube was pumped down to 60 mTorr base pressure, Argon gas (99.995% purity) flow of 250 sccm was used as the carry Se vapor to the reaction zone. The furnace was heated to the growth temperature of 325 °C at the rate of 7 C min^{-1} and held for 1 h (dwell time). After the dwell time, the furnace was allowed to cool down naturally to the room temperature.

Characterization: For *I–V* measurements of the $PdSe_2$ devices, electrical contact was made using another shadow mask which was aligned with the grown $PdSe_2$ channels with the aid of an optical microscope (Olympus BX51M microscope equipped with Jenoptic Progres Gryphax camera). 40 nm thick gold pads were deposited via thermal evaporation. The electrical measurements of the devices were performed in a probe station using a current preamplifier (DL instruments 1211) interfaced with Lab View program under ambient conditions. A tapping mode AFM (Veeco instruments, Dimension 3100) topography was used to determine Pd and $PdSe_2$ film thickness measurements. XPS measurements were carried out using a Thermo Scientific (Escalab Xi) system with a monochromatic Al Kα source in a scan area of 300 × 300 μm^2. Charging effect was calibrated by using standard carbon (C) 1 s peak at 284.8 eV. Confocal Raman measurements were carried out using a Horiba LabRAM HR Evolution Nano system at an excitation wavelength of 532 nm and with laser power < 1 mW in ambient conditions. KPFM measured were performed using the same system in frequency modulation (FM-KPFM) mode with gold coated Si cantilevers. Freshly cleaved HOPG surface was used to calibrate the WF of the cantilever.

Doping of PdSe2 Devices: A reduced BV solution was synthesized and extracted from a biphasic solution of toluene and benzyl viologen dichloride (Sigma-Aldrich) dissolved in water as described by Kim et al.[20] The substrate with patterned $PdSe_2$ devices was exposed to BV by either drop-casting or by immersing in BV solution for doping, the amount doping was monitored up to 12 h. For heterostructure fabrication, doped and undoped regions of the same $PdSe_2$ channel was obtained by covering half of the $PdSe_2$ channel with a PMMA/Au mask and then immersing the substrate in BV solution for 30 min.

Supporting Information

Supporting Information is available from the Wiley Online Library or from the author.

Acknowledgements

This work was supported by the U.S. National Science Foundation (NSF) under grant no. 1728309 and 1920050 (MRI). The authors acknowledge Dr. William Kaden and Dr. Lei Zhai for XPS discussions.

Conflict of Interest

The authors declare no conflict of interest.

Data Availability Statement

Data available on request from the authors.

Keywords

2D materials, $PdSe_2$ thin films, charge transfer doping, electrical transport, van der Waals heterostructures

Received: October 29, 2020
Revised: December 25, 2020
Published online: January 25, 2021

[1] a) G. Cunningham, U. Khan, C. Backes, D. Hanlon, D. McCloskey, J. F. Donegan, J. N. Coleman, *J. Mater. Chem. C* **2013**, *1*, 6899; b) N. Perea-López, A. L. Elías, A. Berkdemir, A. Castro-Beltran, H. R. Gutiérrez, S. Feng, R. Lv, T. Hayashi, F. López-Urías, S. Ghosh, B. Muchharla, S. Talapatra, H. Terrones, M. Terrones, *Adv. Funct. Mater.* **2013**, *23*, 5511.

[2] B. Radisavljevic, A. Radenovic, J. Brivio, V. Giacometti, A. Kis, *Nat. Nanotechnol.* **2011**, *6*, 147.

[3] J. Pu, Y. Yomogida, K.-K. Liu, L.-J. Li, Y. Iwasa, T. Takenobu, *Nano Lett.* **2012**, *12*, 4013.

[4] H. R. Gutiérrez, N. Perea-López, A. L. Elías, A. Berkdemir, B. Wang, R. Lv, F. López-Urías, V. H. Crespi, H. Terrones, M. Terrones, *Nano Lett.* **2013**, *13*, 3447.

[5] A. Castellanos-Gomez, *J. Phys. Chem. Lett.* **2015**, *6*, 4280.

[6] A. D. Oyedele, S. Yang, L. Liang, A. A. Puretzky, K. Wang, J. Zhang, P. Yu, P. R. Pudasaini, A. W. Ghosh, Z. Liu, C. M. Rouleau, B. G. Sumpter, M. F. Chisholm, W. Zhou, P. D. Rack, D. B. Geohegan, K. Xiao, *J. Am. Chem. Soc.* **2017**, *139*, 14090.

[7] X. Chen, X. Lu, B. Deng, O. Sinai, Y. Shao, C. Li, S. Yuan, V. Tran, K. Watanabe, T. Taniguchi, D. Naveh, L. Yang, F. Xia, *Nat. Commun.* **2017**, *8*, 1672.

[8] W. L. Chow, P. Yu, F. Liu, J. Hong, X. Wang, Q. Zeng, C.-H. Hsu, C. Zhu, J. Zhou, X. Wang, J. Xia, J. Yan, Y. Chen, D. Wu, T. Yu, Z. Shen, H. Lin, C. Jin, B. K. Tay, Z. Liu, *Adv. Mater.* **2017**, *29*, 1602969.

[9] a) L.-S. Lu, G.-H. Chen, H.-Y. Cheng, C.-P. Chuu, K.-C. Lu, C.-H. Chen, M.-Y. Lu, T.-H. Chuang, D.-H. Wei, W.-C. Chueh, W.-B. Jian, M.-Y. Li, Y.-M. Chang, L.-J. Li, W.-H. Chang, *ACS Nano* **2020**, *14*, 4963; b) A. D. Oyedele, S. Yang, T. Feng, A. V. Haglund, Y. Gu, A. A. Puretzky, D. Briggs, C. M. Rouleau, M. F. Chisholm, R. R. Unocic, D. Mandrus, H. M. Meyer, S. T. Pantelides, D. B. Geohegan, K. Xiao, *J. Am. Chem. Soc.* **2019**, *141*, 8928; c) A. Di Bartolomeo, A. Pelella, X. Liu, F. Miao, M. Passacantando, F. Giubileo, A. Grillo, L. Iemmo, F. Urban, S.-J. Liang, *Adv. Funct. Mater.* **2019**, *29*, 1902483.

[10] G. Wang, L. Li, W. Fan, R. Wang, S. Zhou, J.-T. Lü, L. Gan, T. Zhai, *Adv. Funct. Mater.* **2018**, *28*, 1800339.

[11] L.-H. Zeng, D. Wu, S.-H. Lin, C. Xie, H.-Y. Yuan, W. Lu, S. P. Lau, Y. Chai, L.-B. Luo, Z.-J. Li, Y. H. Tsang, *Adv. Funct. Mater.* **2019**, *29*, 1806878.

[12] L.-B. Luo, D. Wang, C. Xie, J.-G. Hu, X.-Y. Zhao, F.-X. Liang, *Adv. Funct. Mater.* **2019**, *29*, 1900849.

[13] a) M. Long, Y. Wang, P. Wang, X. Zhou, H. Xia, C. Luo, S. Huang, G. Zhang, H. Yan, Z. Fan, X. Wu, X. Chen, W. Lu, W. Hu, *ACS Nano* **2019**, *13*, 2511; b) L.-H. Zeng, Q.-M. Chen, Z.-X. Zhang, D. Wu, H. Yuan, Y.-Y. Li, W. Qarony, S. P. Lau, L.-B. Luo, Y. H. Tsang, *Adv. Sci.* **2019**, *6*, 1901134.

[14] a) Y. Gao, X. Liu, W. Hu, J. Yang, *Phys. Chem. Chem. Phys.* **2020**, *22*, 12973; b) S.-H. Zhang, B.-G. Liu, *J. Mater. Chem. C* **2018**, *6*, 6792.

[15] X. Zhang, Z. Shao, X. Zhang, Y. He, J. Jie, *Adv. Mater.* **2016**, *28*, 10409.

[16] D. Kiriya, M. Tosun, P. Zhao, J. S. Kang, A. Javey, *J. Am. Chem. Soc.* **2014**, *136*, 7853.

[17] P. Luo, F. Zhuge, Q. Zhang, Y. Chen, L. Lv, Y. Huang, H. Li, T. Zhai, *Nanoscale Horiz.* **2019**, *4*, 26.
[18] a) Y. Zhan, Z. Liu, S. Najmaei, P. M. Ajayan, J. Lou, *Small* **2012**, *8*, 966; b) C. H. Mak, S. Lin, L. Rogée, S. P. Lau, *J. Phys. D: Appl. Phys.* **2019**, *53*, 065102.
[19] F. A. Rasmussen, K. S. Thygesen, *J. Phys. Chem. C* **2015**, *119*, 13169.
[20] S. M. Kim, J. H. Jang, K. K. Kim, H. K. Park, J. J. Bae, W. J. Yu, I. H. Lee, G. Kim, D. D. Loc, U. J. Kim, E.-H. Lee, H.-J. Shin, J.-Y. Choi, Y. H. Lee, *J. Am. Chem. Soc.* **2009**, *131*, 327.
[21] S. Zhao, Z. Li, G. Wang, J. Liao, S. Lv, Z. Zhu, *RSC Adv.* **2018**, *8*, 11070.
[22] N. Peimyoo, W. Yang, J. Shang, X. Shen, Y. Wang, T. Yu, *ACS Nano* **2014**, *8*, 11320.
[23] a) A. N. Hoffman, Y. Gu, L. Liang, J. D. Fowlkes, K. Xiao, P. D. Rack, *npj 2D Mater. Appl.* **2019**, *3*, 50; b) Q. Liang, Q. Zhang, J. Gou, T. Song, H. C. Arramel, M. Yang, S. X. Lim, Q. Wang, R. Zhu, N. Yakovlev, S. C. Tan, W. Zhang, K. S. Novoselov, A. T. S. Wee, *ACS Nano* **2020**, *14*, 5668.
[24] a) Y. Tan, H. Wang, P. Liu, Y. Shen, C. Cheng, A. Hirata, T. Fujita, Z. Tang, M. Chen, *Energy Environ. Sci.* **2016**, *9*, 2257; b) Q. Wang, K. Cui, J. Li, Y. Wu, Y. Yang, X. Zhou, G. Ma, Z. Yang, Z. Lei, S. Ren, *Nanoscale* **2020**, *12*, 9171.
[25] J. Meyer, P. R. Kidambi, B. C. Bayer, C. Weijtens, A. Kuhn, A. Centeno, A. Pesquera, A. Zurutuza, J. Robertson, S. Hofmann, *Sci. Rep.* **2014**, *4*, 5380.
[26] K. H. Kim, K. S. Kim, Y. J. Ji, I. Moon, K. Heo, D.-H. Kang, K. N. Kim, W. J. Yoo, J.-H. Park, G. Y. Yeom, *J. Mater. Chem. C* **2020**, *8*, 1846.
[27] W. Chen, C. Tang, T. Li, X. Zou, J. Zhang, S. Jia, J. Yuan, A. George, D. Voronine, P. Ajayan, Q. Li, L. Hao, J. Lou, *Extreme Mech. Lett.* **2020**, *41*, 100996.
[28] N. Kang, C. W. Smith, M. Ishigami, S. I. Khondaker, *Appl. Phys. Lett.* **2017**, *111*, 233303.

